

Resolving Globular Cluster Formation within a Cosmological Context

Aaron C. Boley, George Lake, Justin Read, & Romain Teyssier

Institute for Theoretical Physics, University of Zurich, Winterthurerstrasse 190, Zurich, CH-8057, Switzerland; aaron.boleym@gmail.com

ABSTRACT

We place constraints on the formation redshifts for blue globular clusters (BGCs), independent of the details of hydrodynamics and population III star formation. We argue that BGCs and stellar halos have a common origin and that simulations of 1 Mpc boxes up to $z \sim 10$ must resolve BGC formation. We present a proof-of-concept simulation that captures the formation of globular-like star clusters.

Subject headings: cosmology: early universe – galaxies: star clusters – stars: population II

1. Introduction

The first stars and star clusters are responsible for the initial chemical enrichment of the universe. They are signatures of the earliest stages of galaxy formation, and their remnants may provide the seeds for supermassive black holes. The oldest known star clusters are globular clusters (GCs). Their color distribution is bimodal (Zinn 1985; Harris 2009), possibly indicating two formation channels. The blue, metal-poor GCs ($[\text{Fe}/\text{H}] < -1$) have a typical $[\text{Fe}/\text{H}] \sim -1.5$ and the red, metal-rich ($[\text{Fe}/\text{H}] > -1$) population has a typical $[\text{Fe}/\text{H}] \sim -0.5$. Blue GCs (BGCs) have chemical signatures and radial distributions that are similar to halo stars (e.g., Helmi 2008), while the red population is associated with the galactic disk and shows a clear circular velocity component. Relative age estimates indicate that red GCs are younger than BGCs, with an average age separation of about 1.5 Gyr between the Galactic populations (e.g., de Angeli et al. 2005). The typical GC in the Galaxy has an $M_V \sim -7.3$ (Harris 1991) and mass $M = 1.4 \times 10^5 M_\odot$, assuming a mass-to-light ratio $\Upsilon = 2$. The dark matter content of these systems is small, if present at all (e.g., Moore 1996; Baumgardt et al. 2009).

Theoretically, the formation of GCs remains poorly understood. Peebles & Dicke (1968) argued that cloud condensates could form shortly after recombination, preceding protogalaxy formation. Gunn (1980) and McCrea (1982) suggested that compression behind strong shocks, e.g., during mergers, could create clouds with Jeans masses $\sim 10^6 M_\odot$. Fall & Rees (1985) found that gas clouds with temperatures $\sim 10^4$ K could condense out of a $\sim 10^6$ K gas via a thermal instability and that, if the cooling of these clouds were to stall at 10^4 K, the corresponding cloud mass would be $\sim 10^6 M_\odot$. Ashman & Zepf (2001) treated molecular clouds as Bonnor-Ebert-like objects and argued that the increase in ISM pressure during a major merger can compress molecular clouds to radii ~ 6 pc, which might produce GCs rather than open clusters and associations. A summary of various formation scenarios is given by Brodie & Strader (2006).

Moore et al. (2006) showed that the radial distribution of dark matter that collapsed into halos by $z \sim 12$, with mass scales $\gtrsim 2.5\sigma(M, z)$, is consistent with the radial distribution of the Galaxy’s BGCs and halo stars. This argues, along with estimated ages (e.g., Sarajedini et al. 2007), that BGC formation may be best understood within a cosmological context. Bromm & Clarke (2002) investigated whether GCs can form during the formation of protodwarf galaxies ($\sim 10^8 M_\odot$), and identified gas clumps in their simulation with masses $\sim 10^6 M_\odot$. Kravtsov & Gnedin (2005) also used cosmological simulations and a subgrid model to form cluster particles in dwarf galaxies with $M > 10^9 M_\odot$. However, none of these simulations has demonstrated that GCs do form, nor has one demonstrated why a $10^6 M_\odot$ cloud should form a GC at high z , while such clouds form associations or open clusters today.

Halo stars are also old, but their connection with BGC formation remains uncertain. These stars have abundance distributions that are similar to BGCs, and do not have an obviously different radial bias (e.g., Brodie & Strader 2006; Helmi 2008). In the Galaxy, the cluster mortality rate is known to be high (Lada & Lada 2003; Bastian & Goodwin 2006), and the destruction of star clusters that formed along with BGCs could produce a substantial fraction of the halo. Fall & Zhang (2001) showed that a power law initial cluster luminosity function (ICLF), like what is seen in the Antennae (Schweizer 1987; Zhang & Fall 1999), could be shaped into the globular cluster luminosity function (GCLF).

This paper focuses on the formation of BGCs using arguments that are independent of the details of hydrodynamics and star formation. We show that halo stars and BGCs could have a common origin; we place constraints on the epoch of halo star and BGC formation; and, we argue that simulations of a biased region of the universe, with box sizes ~ 1 Mpc comoving, should capture BGC formation by $z \sim 10$, regardless of the mechanism. In §2, we estimate the mass of the halo star population in the Milky Way Galaxy (MWG) by combining the GCLF with an ICLF. We then find the maximum redshift that BGC and halo

star formation could have been completed in §3. In §4, we use radial biasing to constrain star formation efficiencies. We present in §5 a proof-of-concept simulation of the formation of star clusters at high z . Our conclusions are summarized in §6.

2. Luminosity Functions and Mass Estimates

In this section, we calculate the total mass that MWG halo stars and BGCs would have if they formed in an Antennae-like initial cluster mass function (ICMF). The GCLF $\Phi \propto \exp(-(V - V_0)^2/2\sigma_V^2)$, for absolute visual magnitude V and turnover magnitude V_0 . The globular cluster mass function (GCMF) can be estimated by assuming a constant mass-to-light ratio Υ : $f_{GC} \propto \exp(-(\mu - \mu_0)^2/2\sigma_\mu^2)$, where $\mu = \log m$ for mass m . We set $V_0 = -7.3$ and $\sigma_V = 1.2$, which is consistent with the Harris (1991) and Gnedin (1997) fits for MWG GCs. Assuming $\Upsilon = 2$ gives $\mu_0 = 5.15$ and $\sigma = 0.48$. We normalize the mass function to the Milky Way’s BGC population, which we take to be $N_{GC} \sim 100$. To represent the ICMF, we use the results from Zhang & Falls (1999), who found that the $f_{SC} = mdN/dm \propto m^{1-\beta}$, with $\beta \sim 2$. Figure 1 shows curves for f_{GC} and f_{SC} , where f_{SC} is normalized such that it osculates with f_{GC} at $\mu_{osc} = \mu_0 + 2.3\sigma_\mu^2$. Integrating f_{SC} yields a total mass of $104m_{osc}(\mu_{high} - \mu_{low})$. Including star clusters between -2 and $-12 V$, the total mass in the power law distribution is $2 \times 10^8 M_\odot$, compared with 2.6×10^7 for the present-day BGCs.

The above argument accounts for reshaping the ICMF into the GCMF through cluster destruction. Not only should the slope change due to the loss of low-mass clusters, but evaporation should change the peak of the resulting GCMF. Gnedin & Ostriker (1997) found typical GC destruction rates of 0.03/Gyr and 0.1/Gyr for evaporation and evaporation+disk-shocking, respectively. For simplicity, we assume that these rates are constant, which reduces the mass function by a factor of 1.5 or 4, respectively, over 13 Gyr. Therefore the mass in halo stars that could be produced during BGC formation is between 3 and $8 \times 10^8 M_\odot$, consistent with estimates of the stellar halo mass (e.g., Binney & Tremaine 2008).

Other authors have investigated whether the halo population could be produced by dissolved clusters. For example, Surdin (1995) completed a similar calculation to ours, but concluded that cluster dissolution was nonviable (see also Ostriker & Gnedin 1997). His conclusion was based on comparing the mass of dissolved clusters to the mass of the entire spheroid (bulge+halo; $\sim 5 \times 10^9 M_\odot$). However, the bulge population is chemically different from the stellar halo. Zoccali et al. (2003) found that the peak of the metallicity distribution in the bulge is $[\text{Fe}/\text{H}] \sim -0.1$ and extends to ~ -1 , while the halo has a peak $[\text{Fe}/\text{H}] \sim -1.6$ and extends to about ~ -3 (Helmi 2008), similar to BGCs (Zinn 1985). The mass in bulge stars could be formed well after halo star formation. Its mass is not included in our estimate.

Our calculation demonstrates that the halo star population could have come from dissolved clusters that formed along with the present-day BGCs; we assume this scenario for the rest of the paper. For this estimate, we used an Antennae-like ICMF. It is unclear whether this profile describes the distribution of star clusters at high z , but the detailed shape of the ICMF is not central to our argument. We only require that a distribution of clusters is produced along with the BGCs, and an Antennae ICMF gives us a reasonable model. We find a minimal extrapolated mass of $2 \times 10^8 M_\odot$. Including cluster evaporation, the mass in halo stars produced during BGC formation is consistent with $3\text{--}8 \times 10^8 M_\odot$. Hereafter, we assume this mass to be $M_h \sim 5 \times 10^8 M_\odot$, consistent with observational constraints on the MWG’s stellar halo.

3. Required Star Formation Efficiency

In this section, we estimate the maximum redshift that BGC formation could have been completed using the conditional mass function (Press & Schechter 1974; Zentner 2007) with the Sheth & Tormen (2002) formalism. We set the critical density for collapse $\delta_c = 1.686$. The value for a density fluctuation δ for a given z is determined by scaling δ_c with the Carroll et al. (1992) growth function. The mass variance is calculated using a real space filter. We use the Eisenstein & Hu (1998) transfer function with baryonic acoustic oscillations. The conditional mass function can be integrated to find the fraction of mass in halos with $M \geq M_{\min}$ at z that will be included in a halo of mass M_0 at z_0 .

We take $M_0 = 10^{12} M_\odot$ at $z_0 = 0$, and assume WMAP 5 cosmology ($\Omega_c = 0.214$, $\Omega_b = 0.044$, $\Omega_\Lambda = 0.742$, and $h = 0.719$; Hinshaw et al. 2009). The slope of the power spectrum $n = 0.95$, and $\sigma_8 = 0.8$. The minimum mass for a halo M_{\min} is set by the lowest mass we expect to be relevant to BGC formation. This mass must be $\gtrsim 10^6 M_\odot$, i.e., where we expect the first stars to form. Figure 2 shows the cumulative baryon mass in collapsed objects, assuming the universal baryon fraction, for minimum dark matter halo masses of 10^6 , 10^7 , 10^8 , and $10^9 M_\odot$. The three thin horizontal lines indicate the mass fraction in baryons required to form $\sim 5 \times 10^8 M_\odot$ of halo stars and BGCs, assuming a global star formation efficiency (SFE) of $\eta = 1\%$ (top), 10% (middle), and 24% (bottom). The latter is the global SFE that is required to form all the stars in the MWG, assuming a universal baryon fraction and a total mass in stars $\sim 5 \times 10^{10} M_\odot$. The gray region indicates the reionization redshift, based on WMAP5 results. The plot indicates that halo star and BGC formation could have been completed before reionization for SFEs $\sim 10\%$, if BGC formation took place in halos less massive than $10^8 M_\odot$. However, we must also address whether enough mass was available in biased halos.

4. Radial Biasing Constraints

Diemand et al. (2005) and Moore et al. (2006) used dark matter simulations to demonstrate that material that collapses into halos with mass scales of $\nu \gtrsim 2.5$ at high redshift, where $\nu = \delta_c/\sigma(M, z)$, has a radial distribution in the $z = 0$ galaxy that is consistent with the MWG halo stars’ and BGCs’. We note that the characteristic mass, i.e., the knee in the Press-Schechter function, corresponds to $\nu = \sqrt{6}$ (Binney & Tremaine 2008). Using the Sheth-Tormen conditional mass function, we integrate over all halos with masses greater than $\sigma(M, z)$ for $\nu = 2.5$. At $z \sim 12$, this mass fraction $f_{\nu \geq 2.5} \sim 0.027$, which is delineated by the thick, solid line in Figure 2. In order to produce the halo and BGC population from exclusively high- ν halos, the global SFE needs to be $\gtrsim 10\%$. We analyzed the Diemand et al. simulation data for comparison with the Sheth-Tormen formalism. We reproduced the biasing results, but noted that more collapsed objects were found in the simulations than predicted by the conditional mass function for $z \gtrsim 5$. The biased mass as calculated from Sheth-Tormen may be a lower limit.

For a 10% SFE, about 10% of halo stars and BGCs could be produced by $z \sim 18$ and the earliest formation can end is $z \sim 13$. This redshift interval corresponds to about 120 Myr. The Lagrangian volume for the MWG is approximately 27 Mpc^3 comoving. Using these figures, we estimate the star formation rate required to form $5 \times 10^8 M_\odot$ of stars is $\sim 0.15 M_\odot \text{ yr}^{-1} \text{ Mpc}^{-3}$. This value is similar to the observed peak in the universal star formation rate (Madau et al. 1998; 0.12-0.17 $M_\odot \text{ yr}^{-1} \text{ Mpc}^{-3}$ at $z \sim 1.5$). If BGC formation extends to $z \sim 10$, our estimate would be about a factor of two lower. Note that the universe is only about 500 Myr old by $z \sim 10$; de Angeli et al. (2005) report an age spread in their low-metallicity GC sample that is less than 600 Myr and is consistent with an age spread of zero.

In order to investigate the formation of halo stars and BGCs using numerical techniques, only a small, biased box needs to be simulated. For the considered cosmology, a simulation of a 1 Mpc comoving box should capture BGC formation by $z \sim 10$, which is about the turnaround redshift, regardless of the underlying process. Based on the Sheth-Tormen mass function, the simulation volume should contain three $10^8 M_\odot$ halos by the end redshift. If BGCs do not form in such a simulation, there is likely a problem with the subgrid model that is employed.

5. Test Simulation

5.1. Setup

We highlight preliminary simulation results, which will be presented in detail in a forthcoming paper. We employ RAMSES (Teyssier 2002) in order to simulate the formation of the first star clusters. RAMSES is an adaptive mesh refinement cosmology code that solves the equations of hydrodynamics using a second-order unsplit Godunov method and integrates particles using particle-mesh techniques. The code has been modified to follow nonequilibrium chemistry for a nine-species gas: e, HI, HII, HeI, HeII, HeIII, H⁻, H₂, and H₂⁺. Cooling due to collisions between H₂ and the other species is modeled according to Glover & Abel (2008).

The Dubois & Teyssier (2008) star formation recipe is modified in order to capture pop III star formation and supernova feedback. Wherever the gas number density is greater than the critical value $n_0 = 10^5 \text{cm}^{-3}$, there is a chance to form a star particle. The local SFE is set to 1% of the cell’s free-fall time $t_{ff} = (3\pi/32G\rho)^{1/2}$. If the metallicity of the gas is above $Z_{\text{thresh}} = 5 \times 10^{-6} Z_{\odot}$, the resulting star particle represents a distribution of population II stars. Ten percent of the of the star particle’s mass is injected back into medium after 10 Myr as supernova ejecta with a metallicity of 0.1. Below Z_{thresh} , the particles represent a distribution of population III stars.

The IMF for population III stars remains unclear. The minimum mass is thought to be $\gtrsim 10M_{\odot}$ (e.g, Glover 2005; Bromm et al. 2009), but this remains highly uncertain. Likewise, the maximum mass for a pop III star is unknown, nor is it known how important pair-instability supernovae were to the enrichment of the second generation of stars. For example Tumlinson et al. (2004) argue that the observed element ratios of old pop II stars are inconsistent with enrichment by pair-instability supernovae. Moreover, the IMF shows little sensitivity to the metallicity (Kroupa 2001). Whether this extends down to extremely low metallicities remains unknown. In the absence of better constraints on pop III star formation, we assume a Salpeter IMF ($dN/dM \sim M^{-2.35}$) with a low-mass cutoff M_{co} (see below). Whenever a star particle is formed, the particle’s mass M_{sp} is distributed among a random distribution of stars. The probability that a star is between masses M_0 and M_1 is given by $P = A(M_1^{-1.35} - M_0^{-1.35})$, where $A = (M_{\text{top}}^{-1.35} - M_{\text{co}}^{-1.35})^{-1}$ and $M_{\text{top}} = 1000M_{\odot}$ is the most massive star in the distribution. A given star mass is selected by setting $M_{\text{star}} = (r/A + M_{\text{co}}^{-1.35})^{-1/1.35}$, where r is a random variable with an even distribution between 0 and 1. This process continues until the total mass in stars is equal to M_{sp} . We set $M_{\text{co}} = 3M_{\odot}$, which is based on the results of Nakamura & Ememura (2001), who find that the smallest Jeans mass for which the gas becomes opaque to H₂ lines is $\sim 1M_{\odot}$.

For each population III star in the distribution, its contribution to ejecta, metal enrichment, long-lived stars and remnants, pair-instability supernovae, and black holes is tracked. Table 1 summarizes the outcome for different stellar masses. The remnant neutron star or black hole mass is determined, when applicable, by $M_{\text{R/BH}} = \text{MAX}(M_{\text{star}} 0.1^{13.5M_{\odot}/M_{\text{star}}}, 1.35M_{\odot})$. This prescription roughly follows the results of Timmes et al. (1996) for population III stellar remnants. Metal enrichment is included using $Z = 0.4(M_{\text{star}} - 13.5M_{\odot})/M_{\text{ejecta}}$ (Woosley & Weaver 1982). Whenever a supernova occurs, for either population II or III, $M_{\text{ejecta}} 10^{50} \text{erg } M_{\odot}^{-1}$ is deposited directly into the cell containing the star.

We use a box size of $589 h^{-1} \text{ kpc}$, and the cosmology is set to $h = 0.719$, $\Omega_{\text{matter}} = 0.258$, $\Omega_{\Lambda} = 0.742$, and $\Omega_b = 0.045$. The power spectrum normalization is set to $\sigma_8 = 1.0$. The box size is smaller than recommended above, but it is intended to be a proof-of-concept simulation. The highest refinement at a given expansion factor a is kept at a physical resolution $\Delta x_{\text{min}} \sim 0.5 \text{ pc}$, which corresponds to refinement level $l = 17$ at $z \sim 13$. For dark matter particles only, the highest level of refinement used in the cloud-in-cell approximation is $l = 13$ in order to avoid two-body relaxation effects (e.g., Knebe et al. 2000; Levine et al. 2008). The initial conditions were generated using the COSMICS package (Bertschinger 1995). The simulation box has a 256 cubed region ($236 h^{-1} \text{ kpc}$) nested within a coarser 128 cubed grid. The dark matter particle mass in the higher resolution region is about $1000 M_{\odot}$.

5.2. Simulation Results

Figure 3 shows maps of the average number density and temperature along the line of sight in a 360 pc cubed region at $z \sim 13.3$. The region contains a $5.3 \times 10^6 M_{\odot}$ dark matter halo with about $10^6 M_{\odot}$ of gas within $R_{200} \sim 420 \text{ pc}$. Two star clusters are present in this halo, with a combined mass $\sim 9 \times 10^4 M_{\odot}$. Most of this mass is in pop II stars, but about $138 M_{\odot}$ is from the pop III generation, either trapped in neutron stars or in stars that will become white dwarfs. Although pop III black holes were not formed in these clusters, some clusters in the simulation have a total black hole mass $\gtrsim 1000 M_{\odot}$. The initial enrichment for the stars in Figure 3 was set by $\sim 190 M_{\odot}$ of pop III stars. Population II stars then formed and enriched new stars in the cluster (Morgan & Lake 1989). This sequence created the distribution shown in the bottom-left panel, with a peak $[\text{Fe}/\text{H}] \sim -1.3$. More than half of the combined mass occurred in a burst of star formation that lasted about $\sim 30 \text{ Myr}$. The effects of supernovae on the surrounding gas can be seen in the temperature and density plots, where bubbles have formed. The simulation demonstrates that the formation of star clusters and their subsequent evolution can be captured from cosmological initial

conditions. If these clusters survive to be called BGCs today, they represent a mode of GC formation that takes place in dark matter minihalos. This formation channel could operate until reionization limits cooling. Cluster formation may then be delayed until massive disk galaxies form, which may be responsible for the red GC population.

6. Conclusions

Taking into account cluster evaporation, we find that about 3×10^8 to $8 \times 10^8 M_\odot$ of stars could have been produced during BGC formation. This indicates that a large fraction, if not most, of the halo stars could be remnants from destroyed BGCs and lower mass clusters that formed with BGCs. Using the conditional mass function, we showed that the entire halo population could be produced by $z \sim 13$ with star formation efficiencies $\sim 10\%$. Based on constraints from reionization, radial biasing, and Press-Schechter theory, we argue that a simulation of a biased, 1 Mpc comoving region of the universe should capture the formation of BGCs by $z \sim 10$. If such a simulation does not capture the formation of these systems, it most likely reflects a problem in the subgrid model or cosmology. Finally, we have presented a simulation that shows the formation of BGC-like clusters with masses $\sim 5 \times 10^4 M_\odot$ by $z \sim 13$. These clusters form in dark matter minihalos and can self-enrich quickly to metallicities that are consistent with BGCs.

This research was supported by an SNF Grant and the University of Zurich. Simulations were run on the zbox2 and zbox3 machines, maintained by ITP UZH. We thank Ben Moore and Joachim Stadel for useful discussions and for making the Diemand et al. data available to us.

REFERENCES

- Ashman, K. M., & Zepf, S. E. 2001, *ApJ*, 122, 1888
- Bastian, N., & Goodwin, S. P. 2006, *MNRAS*, 369, L9
- Baumgardt et al. 2009, arXiv:0904.3329v1
- Bertschinger, E. 1995, arXiv:astro-ph/9506070
- Binney, J., & Tremaine, S. 2008, *Galactic Dynamics*, 2nd ed. (Princeton University Press)
- Brodie, J. P., & Strader, J. 2006, *AR&AA*, 44, 193

- Bromm, V., & Clarke, C. J. 2002, *ApJ*, 566, L1
- Bromm, V., Yoshida, N., Hernquist, L., McKee, C. F. 2009, *Nature*, 459, 49
- Carroll, S. M., Press, W. H., & Turner, E. L. 1992, *ARAA*, 30, 499
- de Angeli et al. 2005, *AJ*, 130, 116
- Diemand, J., Madau, P., & Moore, B. 2005, *MNRAS*, 364, 367
- Dubois, Y., & Teyssier, R. 2008, *A&A*, 477, 79
- Eisenstein, D. J., & Hu, W. 1998, *ApJ*, 496, 605
- Fall, M. S., & Rees, M. J. 1985, *ApJ*, 298, 18
- Fall, S. M., & Zhang, Q. 2001, *ApJ*, 561, 751
- Glover, S. 2005, *Space Sci. Reviews*, 117, 445
- Glover, S. C., & Abel T. 2008, *MNRAS*, 388, 1627
- Gnedin, O. Y. 1997, 487, 663
- Gunn, J. E. 1980, in *Globular Clusters*, ed. D. Hanes & B. Madore (Cambridge: Cambridge Univ. Press), 301
- Harris, W. E. 1991, *ARA&A*, 29, 543
- . 2009, *ApJ*, in press (arXiv:0904.4208)
- Helmi, A. 2008, *Astron. Astrophys. Rev.*, 15, 145
- Hinshaw et al. 2009, *ApJS*, 180, 225
- Knebe, A., Kravtsov, A. V., Gottöber, S., & Klypin, A. A. 2000, *MNRAS*, 317, 630
- Kravtsov, A. V., & Gnedin, O. Y. 2005, *ApJ*, 623, 650
- Kroupa, P. 2001, *MNRAS*, 322, 231
- Lada, C. J., & Lada, E. A. 2003, *ARA&A*, 41, 57
- Levine, R., Gnedin, N. Y., Hamilton, A. J. S., Kravtsov, A. V. 2008, *ApJ*, 678, 154
- Madau, P., Pozzetti, L., & Dickinson, M. 1998, *ApJ*, 498, 106

- McCrea, W. H. 1982, in *Progress in Cosmology*, ed. A. W. Wolfendale (Dordrecht: Reidel), 239
- Moore, B. 1996, *ApJ*, 461, L13
- Moore, B., Diemand, J., Madau, P., Zemp, M., & Stadel, J. 2006, *MNRAS*, 368, 563
- Morgan, S., & Lake, G. 1982, *ApJ*, 339, 171
- Nakamura, F., & Umemura, M. 2001, *ApJ*, 548, 19
- Ostriker, J. P., & Gnedin, O. Y. 1997, 487, 667
- Peebles, P. J. E., & Dicke, R. H. 1968 *ApJ*, 154, 891
- Press, W. H., & Schechter, P. 1974, *ApJ*, 187, 425
- Sarajedini et al. 2007, *AJ*, 133, 1658
- Schweizer, F. 1987, in *Nearly Normal Galaxies: From the Planck Time to the Present* (New York, Springer-Verlag), 18
- Sheth, R. K., & Tormen, G. 2002, *MNRAS*, 329, 61
- Surdin, V. G. 1995, *Astronomy Letters*, 21, 508
- Teyssier, R. 2002, *A&A*, 385, 337
- Timmes, F. X., Woosley, S. E., & Weaver, T. A. 1996, *ApJ*, 457, 834
- Tumlinson, J., Venkatesan, A., & Shull, J. M. 2004, 612, 602
- Woosley, S. E., Weaver, T. A. 1982, in *Supernovae: A Survey of Current Research*, ed. M. J. Rees and R. J. Stoneham (Dordrecht: Reidel), p. 79
- Zentner, A. R. 2007, *IJMPD*, 16, 763
- Zhang, Q., & Fall, S., M. 1999, *ApJ*, 527, L18
- Zinn, R. 1985, *ApJ*, 293, 424
- Zoccali et al. 2003, *A&A*, 399, 931

Mass Range M_{\odot}	Outcome	t_{SN} (Myr)
< 8	M_{LL}	–
$8 < M < 25$	$M_{LL}, M_{\text{ejecta}}$	10
$25 < M < 35$	$M_{BH}, M_{\text{ejecta}}$	10
$35 < M < 140$	M_{BH}	–
$140 < M < 260$	M_{ejecta}	3
$260 > M$	M_{BH}	–

Table 1: The mass in long-lived stars and remnants, M_{LL} , black holes, M_{BH} , and ejecta mass M_{ejecta} . The remnant mass is determined by $M_{\text{R/BH}} = \text{MAX}(M_{\text{star}}0.1^{13.5M_{\odot}/M_{\text{star}}}, 1.35M_{\odot})$, which is based on the results of Timmes et al. (1996). The ejecta mass is the difference between star’s mass and its remnant. In the case of a pair-instability supernova ($140 < M < 260M_{\odot}$), the ejecta mass is the star’s mass. The third column is the supernova delay time.

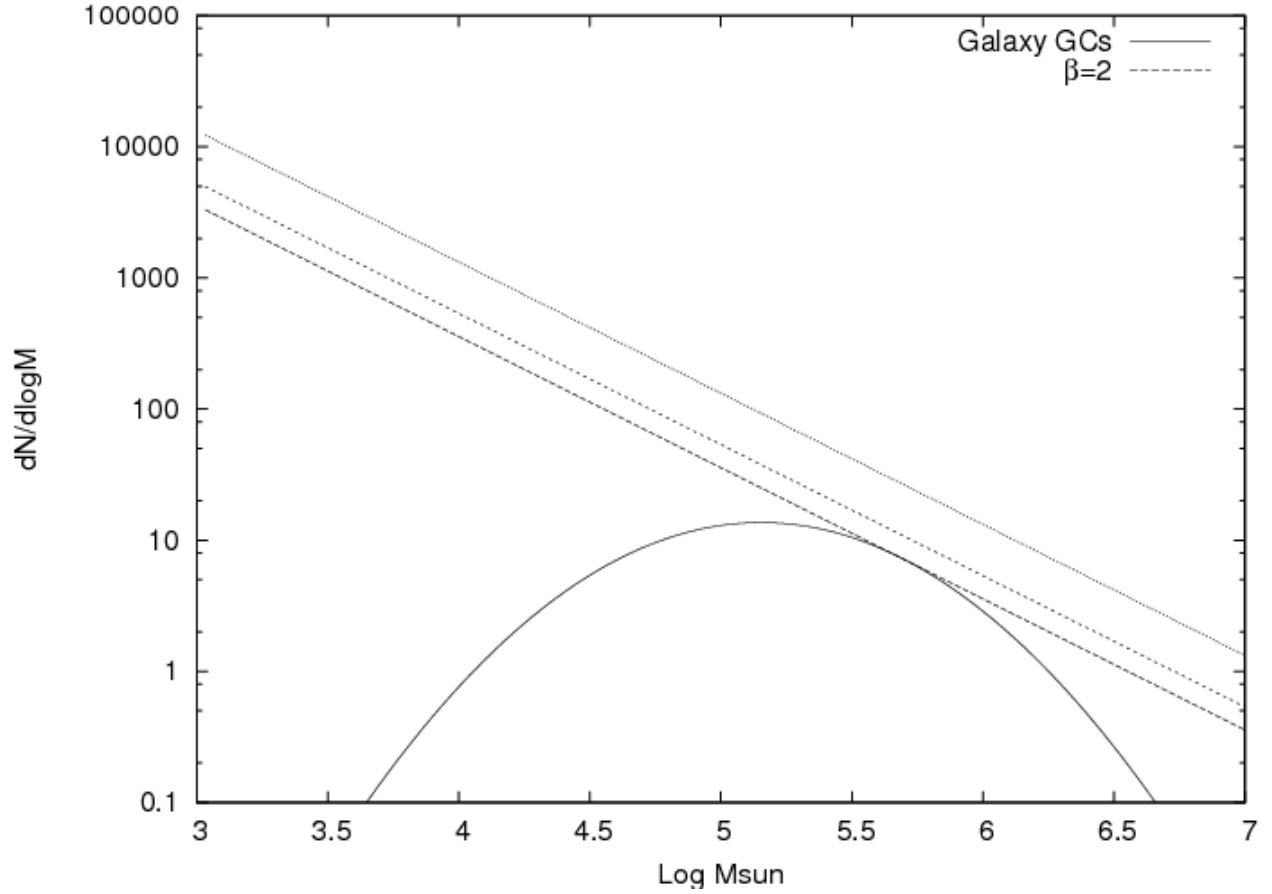


Fig. 1.— The solid curve represents the MWG GCMF, as seen today, normalized by 100 clusters. The lines represent the ICMF $mdN/dm \propto m^{-1}$. The lowest line shows the oscillation mass m_{osc} , the dashed line accounts for evaporation, and the dotted line includes evaporation+disk-shocking.

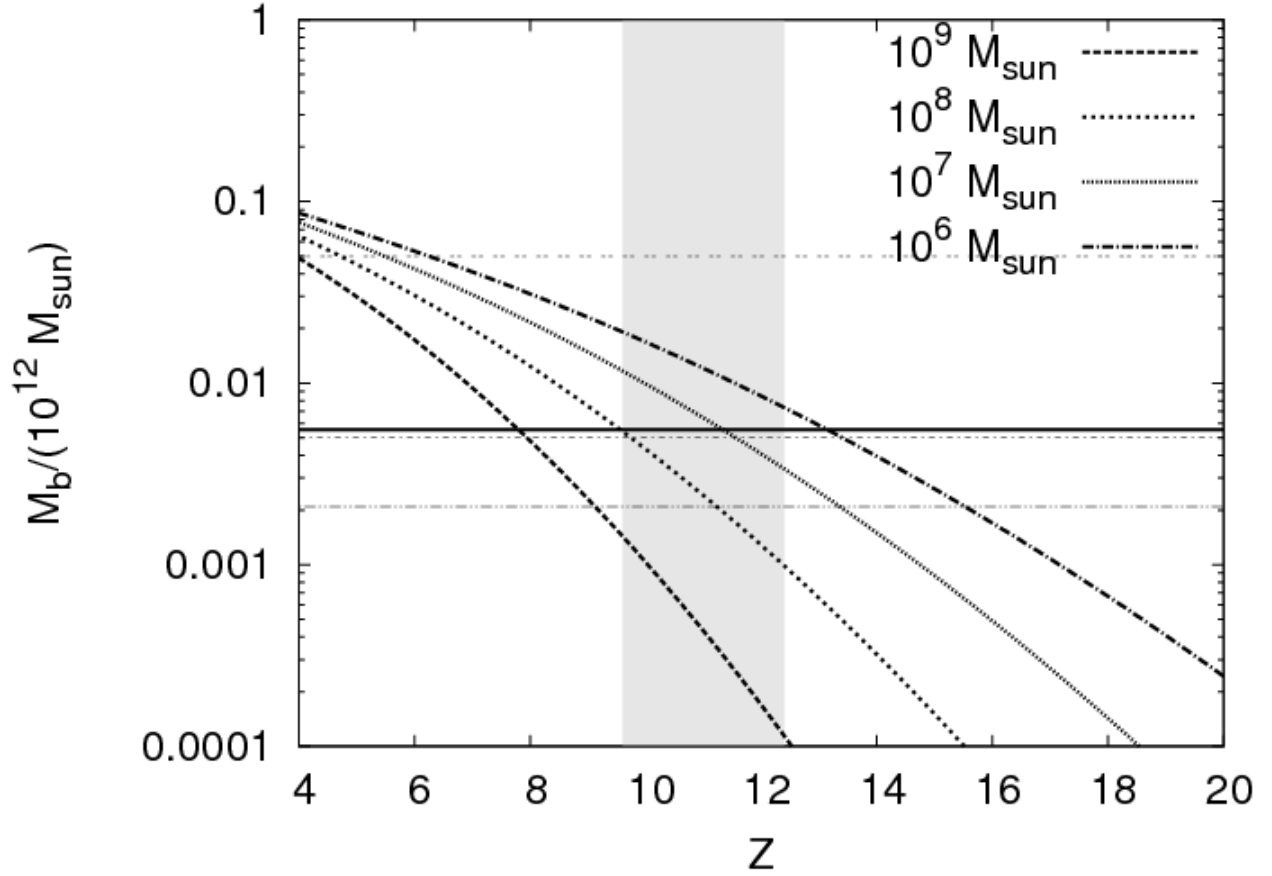


Fig. 2.— Conditional mass function for a halo of $10^{12}M_{\odot}$ at $z = 0$. The curves represent the baryon fraction in collapsed objects for different dark matter halo minimum mass cutoffs. The thin, horizontal lines indicate the baryonic mass that is required to produce $5 \times 10^8 M_{\odot}$ of halo stars and BGCs for a global star formation efficiency of 1%, 10%, and 24%, respectively. The thick line indicates the fraction of mass that comes from $\nu \gtrsim \nu_{2.5}$ (§4). The gray region indicates the WMAP5 measurement for reionization.

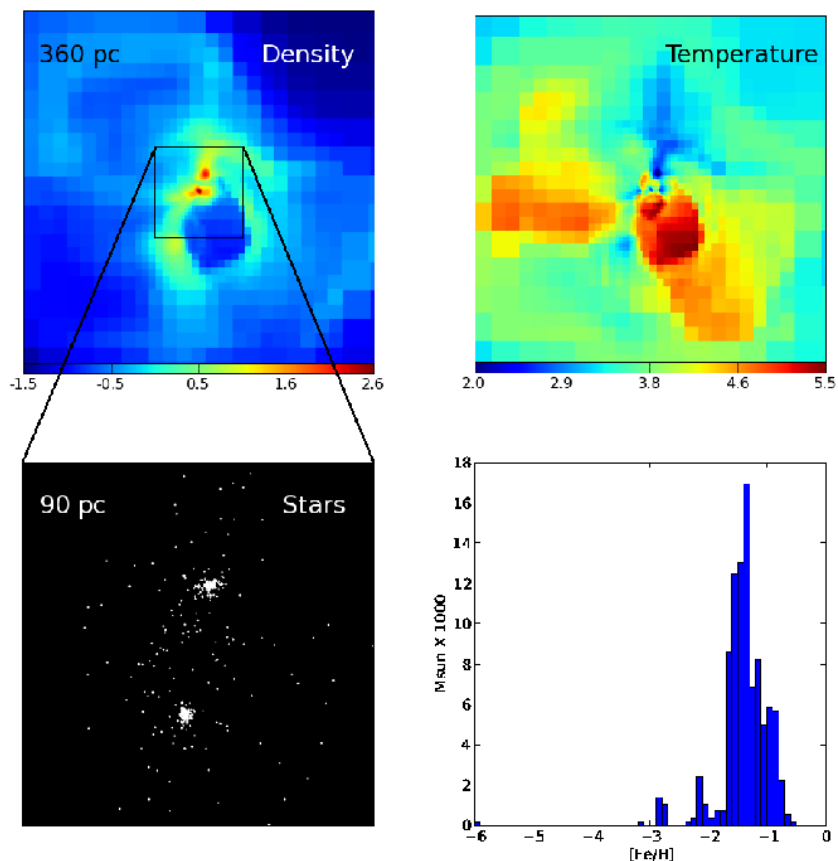


Fig. 3.— Snapshot from a RAMSES simulation with nonequilibrium chemistry and the star formation prescription described in §5. The images correspond to $z \sim 13.3$. Top-left: average number density (cm^{-3}) along the line-of-sight. Top-right: average density-weighted temperature over the mean molecular weight (T/μ K). Bottom-left: star clusters in a dark matter halo $\sim 5 \times 10^6 M_\odot$. Bottom-right: histogram of stellar metallicities for the stars shown in the bottom-left panel.